Journal of Magnetic Resonance **153,** 83–91 (2001)
doi:10.1006/jmre.2001.2418, available online at http://www.idealibrary.com on IDEAL®

Deuterium Stimulated-Echo-Type PGSE NMR Experiments for Measuring Diffusion: Application to a Liquid Crystal

S. V. Dvinskikh,*,[1] I. Furó,*,[2] D. Sandström,† A. Maliniak,† and H. Zimmermann‡

*Division of Physical Chemistry, Department of Chemistry, Royal Institute of Technology, SE-10044 Stockholm, Sweden; †Division of Physical Chemistry, Arrhenius Laboratory, Stockholm University, SE-10691 Stockholm, Sweden; and ‡Max-Planck-Institut für Medizinische Forschung, Department of Biophysics, Jahnstrasse 29, D-69120 Heidelberg, Germany

E-mail: ifuro@physchem.kth.se

Received April 16, 2001; revised July 23, 2001; published online October 5, 2001

The accessibility of molecular self-diffusion coefficients in anisotropic materials, such as liquid crystals or solids, by stimulated-echo-type ^{2}H PGSE NMR is examined. The amplitude and phase modulation of the signal in the stimulated-echo-type sequence by the static quadrupole coupling during the encoding/decoding delays is suppressed by adjusting the pulse flip angles and the phase cycle. For nuclei that experience both nonnegligible quadrupole and dipole couplings, the application of magic echoes during the evolution periods of stimulated echo is demonstrated as a helpful technique in the case of slow diffusion. These findings are demonstrated by experimental results in the thermotropic liquid crystal of partially deuterated 8CB. The obtained diffusion coefficients are also compared to data obtained by a ^{1}H homonuclear-decoupling-type PGSE NMR method in the same material.

Key Words: **^{2}H PGSE NMR; quadrupolar coupling; magic echo; liquid crystal; 8CB.**

INTRODUCTION

Pulsed-field-gradient spin-echo (PGSE) NMR (*1–6*) is a well-established method for studying diffusive molecular motions in isotropic liquids. The technique is based on spatial encoding of the Larmor frequency by applying a strong magnetic field gradient g that, in some other forms of diffusion NMR, can even be static (*7–10*). On increasing g, the observed echo signal A from single-quantum coherences decays as (*1*, *2*)

$$A(g, \delta, \Delta) \propto \exp[-(\gamma g \delta)^2 (\Delta - \delta/3) D], \qquad [1]$$

where the gradient encoding time δ and diffusion time Δ are limited by the transverse and longitudinal relaxation times T_2 and T_1, respectively. As shown by Eq. [1], the sensitivity of the method and the range of accessible diffusion coefficients D for a particular probe design depend on the efficiency of gradient encoding that scales as γ^2, where γ is the magnetogyric ratio. Hence, high-gamma nuclei, such as ^{1}H or ^{19}F, are typically considered as best for NMR diffusion experiments. That should be particularly appropriate in solids and liquid crystals where the PGSE-type diffusion methods developed during the past decade (*7–18*) must often battle with both a small diffusion coefficient D and a short T_2 that strongly limits the time δ available for gradient encoding.

One remedy for nuclei with a nonvanishing static quadrupole or dipole coupling is to excite and encode multiple-quantum coherences (*19–22*) of order n for which the effective gradient becomes ng. In particular, this strategy explored for ^{2}H nuclei could mitigate the effect of the low magnetogyric ratio which, in conventional PGSE experiments, would lead to a gradient encoding ≈40 times less efficient than that for ^{1}H nuclei. Thereby, deuterium PGSE NMR could be extended from the domain of isotropic liquids with more conventional applications such as diffusion of D_2O in solutions of biopolymers and surfactants. Since deuterium is widely used in many complex systems as site-specific and/or chemically selective label this is an important development. Note that the fast diffusion of D_2O in liquid crystal systems has already been investigated by pulsed-field-gradient experiments involving quadrupole echo instead of spin echo (*23–25*).

However, the quadrupolar-echo-type (*23–25*) ^{2}H PGSE NMR has only been explored in anisotropic materials where ^{2}H–^{2}H dipole–dipole interactions were negligible (this interaction is exchange-decoupled in D_2O). The only double-quantum ^{2}H PGSE experiment (*19*) that has been performed to date has demonstrated an advantage in gradient encoding efficiency over its single-quantum counterpart but the potentially negative effect of nonzero dipole–dipole coupling was not investigated. Here we present two new complementary strategies for measuring diffusion by ^{2}H NMR. The first one is the well-known stimulated-echo-type PGSE NMR that has not yet been

[1] On leave from the Institute of Physics, St. Petersburg State University, 198904 St. Petersburg, Russia. Current address: Division of Physical Chemistry, Arrhenius Laboratory, Stockholm University, SE-10691 Stockholm, Sweden.

[2] To whom correspondence should be addressed. Fax: +46 8 790 82 07.

1090-7807/01 $35.00

demonstrated for ^{2}H nuclei in anisotropic systems. The second one is an extension of this approach that includes "magic echo" during gradient encoding/decoding as originally introduced by Zhang and Cory for homonuclear dipole-coupled spin systems (*13*). As demonstrated by results obtained in a partially deuterated thermotropic liquid crystal of 4-octyl-4′-cyanobiphenyl (8CB), these methods, in particular the one with magic echo, are superior to the multiple-quantum strategy. Comparison is also made to a recently developed ^{1}H PGSE NMR method where homonuclear decoupling is applied (*16–18*).

METHODS

Stimulated-Echo-Type ^{2}H PGSE NMR

It is well known that PGSE NMR with stimulated echo (STE, the whole sequence is often abbreviated as PGSTE) performs better than the simple spin echo sequence in systems where $T_2 \ll T_1$ by allowing the diffusion time Δ to extend up to T_1 (recall the increased efficiency of gradient encoding in Eq. [1]). The condition $T_2 \ll T_1$ is often met for dipole-coupled ^{2}H nuclei as those in aliphatic CD_2 or CD_3 groups involved in liquid crystals with slow modes of molecular motion. Hence, the STE-type sequence could replace spin- or quadrupole-echo-type PGSE experiments in analogy with spin $I = \frac{1}{2}$ nuclei. However, the presence of nonzero quadrupole coupling leads to a more complex spin dynamics.

The evolution of an isolated spin $I = 1$ system in the three-pulse sequence of Fig. 1a is governed by the Hamiltonian

$$H = \hbar\omega_Q\left(I_z^2 - \mathbf{I}^2/3\right) - \hbar\omega_i I_z. \qquad [2]$$

with the quadrupole interaction represented by the quadrupole frequency

$$\omega_Q(\theta) = \pm K_Q(3\cos^2\theta - 1)/2, \qquad [3]$$

where K_Q is the strength of the residual quadrupole coupling constant and θ is the orientation of the (axially symmetric) electric field gradient tensor with respect to the applied magnetic field. The spatially dependent offset frequency is defined as

$$\omega_i(z) = \gamma g z, \qquad [4]$$

where g is the strength of field gradient applied in the z direction and $i = 1, 2$ refers to the gradient encoding and decoding periods, respectively.

The spin dynamics during the pulse sequence depicted in Fig. 1a with spin interactions defined as in Eq. [2] is calculated in the Appendix. The sequence with in-phase first and second radiofrequency (RF) pulses, referred to as a cosine sequence, and the sequence with 90° phase shift between the first two pulses, referred to as a sine sequence (*26*), were considered with the RF phases explicitly set to $\{+y, \pm y$, and $\pm y\}$ and to

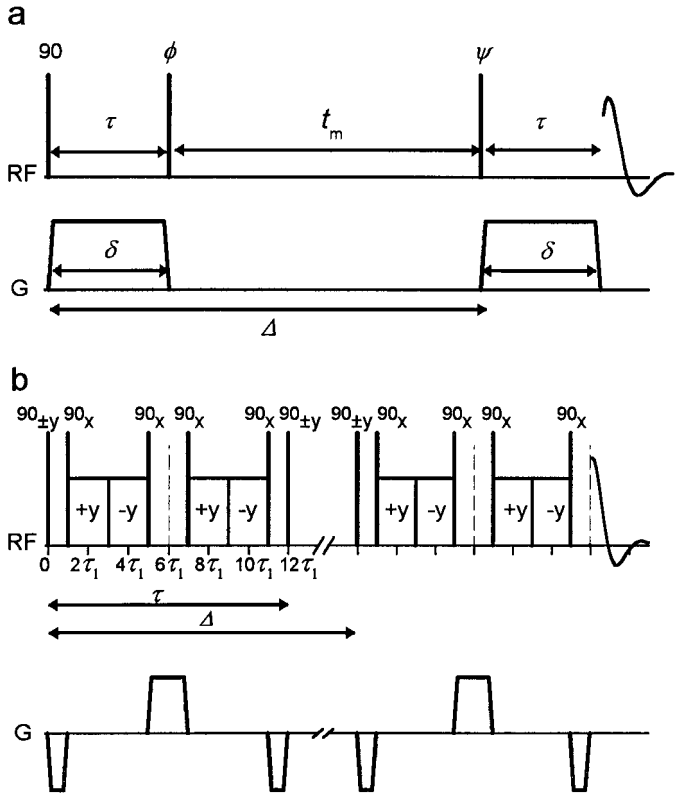

FIG. 1. (a) Stimulated-echo-type PGSE NMR experiment. (b) Stimulated-echo-type PGSE NMR experiment with magic-echo decoupling (*13*).

$\{+y, \pm x$, and $\pm x\}$, respectively, for the first, second, and third pulses. Note that irrespective of the RF phases, both Zeeman and quadrupolar orders (the latter also called spin alignment) are created after the second pulse (except when the pulse angle is $\phi = 90°$) and, consequently, contribute to the signal in both sequences (Eq. [A2]). This is a result of nonzero frequency offset. In contrast, under on-resonance conditions the cosine and sine sequences can be set (by selecting appropriate pulse angles) to excite either Zeeman or quadrupolar orders after the second RF pulse (*26*, *27*).

In a complete analogy to the conventional stimulated echo for spin $I = \frac{1}{2}$ nuclei, the frequency offset is encoded as phase modulation of the detected signal by $(\omega_1\tau)$ and $(\omega_2\tau)$ (Eq. [A4]). An additional complication is the modulation of the signal with (twice) the quadrupole frequency ω_Q that may reduce the overall signal amplitude and distort the phase of the spectrum. These unfavorable features can be avoided through an appropriate choice of the delay τ (see Appendix) that, however, depends on the quadrupole frequency. Hence, this procedure may be impractical if, e.g., the sample orientation or temperature is changed or if deuterons with different quadrupole couplings are present. Moreover, the selected value of τ may be in conflict with the requirements of diffusion encoding/decoding. The quadrupolar modulation can instead be suppressed for an arbitrary quadrupole frequency and frequency offset by adding the

cosine and sine signals recorded at $\phi = \psi = 54.7^\circ$ (Eqs. [A11] and [A12]). In practice, this is achieved by an appropriate phase cycle such as $\{+y, -y, +x, -x\}$ for the second and third RF pulses and $\{-x, -x, +x, +x\}$ for the receiver phase (the phase of the first pulse is fixed to $+y$). This phase cycle compensates simultaneously for the buildup of Zeeman magnetization during t_m. Note that for inequivalent time constants T_{1Q} and T_{1Z} the quadrupolar modulation is reintroduced to some extent for $t_m \sim T_{1Q}, T_{1Z}$.

With the position-dependent offset frequency $\omega_i = \gamma g z$ the total signal is calculated as an integral over the sample volume, which results in (see Eq. [A12])

$$A \sim 2/3 \int m_0 \exp(i(\omega_2 - \omega_1)\tau)\, dz = 2/3\langle \exp(i(\omega_2 - \omega_1)\tau)\rangle, \quad [5]$$

where m_0 is the equilibrium magnetization per unit length in the gradient direction. The offset-dependent factor in Eq. [5] is analogous to that obtained for a conventional stimulated echo sequence for spin $I = \frac{1}{2}$ and, hence, the effect of diffusion reduces to the well-known Stejskal–Tanner formula (*1, 2*)

$$\langle \exp(i(\omega_2 - \omega_1)\tau)\rangle = \exp[-(\gamma g \tau)^2(\Delta - \tau/3)D], \quad [6]$$

where we tacitly assume $\tau = \delta$. Consequently, a diffusion experiment may proceed as for a conventional stimulated echo for spin $I = \frac{1}{2}$. The signal intensity A (in the absence of spin relaxation) is $\frac{1}{3}$ of that after a single 90° pulse (recall that the signal in Eq. [5] is the sum of signals from two experiments), which should be compared to the value of $\frac{1}{2}$ for the conventional stimulated echo sequence for spin $I = \frac{1}{2}$ nuclei. Note that with pulse angles $\phi = \psi = 90^\circ$ and with $\tau = k\pi/\omega_Q$ ($k = 0, 1, 2, \ldots$), one also obtains a signal intensity $A = \frac{1}{2}$ (see Eqs. [A8], [A9]) at the price of quadrupolar modulation.

^{2}H PGSTE NMR with Magic-Echo Decoupling

The presence of static spin interactions other than frequency offset during the encoding/decoding periods of STE-type PGSE diffusion experiments leads to complications as shown in the previous subsection for the case of nonvanishing quadrupole coupling. For nonvanishing multispin dipole–dipole interaction, the primary effect is a fast dipolar dephasing that strongly limits the length of the encoding period δ and thereby the efficiency of gradient encoding that is proportional to δ^2. The latter problem has been dealt with by multiple-pulse dipolar decoupling during encoding/decoding (*16, 18*). Another option is the magic echo (ME) sandwiches (*28*), originally introduced to refocus dipolar dephasing and later demonstrated to be also effective to refocus quadrupolar dephasing (*29*). Combination of ME and field gradient encoding has been used in ^{1}H solid state imaging (*30–35*) and in a ^{19}F PGSE NMR experiment for measuring spin diffusion in rigid solids (*13*).

If nonvanishing quadrupole and multispin dipole–dipole interactions coexist, the situation is more complex. ME sandwiches were shown to provide a good decoupling for this case (*29*). This advantage can only be exploited if there are wide enough windows for inserting gradient pulses. Below, we demonstrate experimentally the validity of this approach.

The pulse sequence (*13*) of a PGSTE NMR experiment with ME decoupling (PGSTE-ME) is shown in Fig. 1b. The echo formation after the magic sandwich is due to the sign reversal of homonuclear dipole and quadrupole interactions during on-resonance RF irradiation, so that the average dipolar and quadrupolar Hamiltonians vanish for the period of $6\tau_1$ (Fig. 1b). Hence, the effective Hamiltonian for the free evolution period $\tau/3$ (see Fig. 1b) becomes (*31, 33–35*)

$$H = -\hbar\omega I_z, \quad [7]$$

where ω is the offset frequency. Gradient pulses, if inserted in windows between RF pulses of the magic sandwich, do not interfere with the refocusing. The sequence actually shown is a combination of ME with 180° inversion pulses, also called mixing echo (*30, 33–35*), that refocuses both linear (e.g., field inhomogeneity and chemical shift) and bilinear spin interactions. To preserve encoding the signs of the inserted gradient pulses are set as indicated (Fig. 1b). Hence, the spin density operator at the end of the encoding period is given by

$$\sigma(\tau) = \exp(i\hbar\gamma g z \delta I_z)\, \sigma(0) \exp(-i\hbar\gamma g z \delta I_z) \quad [8]$$

with gradient time $\delta \leq 4\tau_1 = \tau/3$ ($\sigma(0) \propto I_x$ is the initial density operator generated by the first RF pulse). This equation is analogous to the expression obtained for on-resonance spin $I = \frac{1}{2}$ nuclei in a conventional PGSTE experiment, and therefore the signal is attenuated upon the increasing gradient as given in Eq. [1]. Hence, a PGSTE-ME experiment can proceed by recording the variation of the signal intensity with increasing gradient strength.

Although less than one-third of period τ is available for diffusion encoding by gradient pulses in this ME-based sequence, an efficient refocusing by MEs allows an overall increase (by about one order of magnitude) of τ and thereby a longer effective encoding time, as will be demonstrated below. A potential disadvantage of the PGSTE-ME sequence is heating with consequent temperature shift and gradient by the long RF irradiation that must be carefully controlled. In a ME sandwich the RF "lock" pulses must maintain $\gamma B_1 \geq \omega_Q$. In liquid crystalline samples the quadrupolar coupling $\omega_Q/2\pi$ is partially averaged by fast molecular motions to a value on the order of 10 kHz or below. With $\gamma B_1/2\pi$ on the order of 10 kHz for approximately millisecond pulse lengths, the RF heating can be easily adjusted to $\leq$1 K by the delay between transients (note that the exact figures depend on the conductivity of the sample).

RESULTS AND DISCUSSION

Spectra and Relaxation Rates

The performance of the PGSTE-ME method is demonstrated in a thermotropic liquid crystal 4-octyl-4′-cyanobiphenyl (8CB, see Fig. 2), deuterated in all positions except the β-CH_2 group of the aliphatic chain. The ^{2}H and ^{1}H NMR spectra of the sample in its smectic phase at 300 K and recorded at 31 and 200 MHz, respectively, are shown in Fig. 2. The phase director of the sample is homogeneously oriented along the magnetic field. The assignment of the aliphatic chain was reported previously (*36*) while the assignment of the aromatic part is based on the 2D ^{2}H–^{13}C heteronuclear multiple-quantum correlation spectrum for a homologue sample of 5CB (*37*). The narrowest ^{2}H line with 200 Hz width (at half-height) belongs to the ω-methyl group. In the ^{1}H spectrum the outer doublet is assigned to the two dipole-coupled β-protons, while the central line arises from the residual protons at nominally deuterated positions.

As discussed above, the maximum lengths of the encoding/decoding and diffusion intervals are limited by relaxation times. The experimental values of deuteron relaxation times at selected temperatures and for different deuterium positions in the nematic and smectic phases are collected in Tables 1 and 2. The longitudinal relaxation time, T_1, was estimated from inversion-recovery experiments, while the transverse relaxation time for single-quantum coherences, T_{2SQ}, is defined as the decay constant obtained in the quadrupole echo (*38*) sequence by increasing the echo time. The decay time of the quadrupolar order T_{1Q}, which also influences the echo decay, was not measured but is known to be on the order of the T_{1Z} time (*39*). Having the longest relaxation times, the methyl deuterons are the best suited for measuring the molecular diffusion of 8CB.

In addition, the decay time of double-quantum (DQ) coherences T_{2DQ} was measured for the methyl group (Table 2) by the DQ spin echo pulse sequence (*40–42*). Since the decay was not purely monoexponential, T_{2DQ} was estimated from the time at which the signal reaches the $1/e$ level. Unexpectedly, T_{2DQ} was found to be about 2–4 times shorter than the transverse relaxation time of single-quantum coherences T_{2SQ}. Since this behavior is forbidden for isolated deuterons (*40, 43*), for which theory predicts T_{2DQ} on the order of T_1 time, the decay of the DQ coherences in the present sample must be dominated by dipolar effects (*41, 44–46*). On the other hand, the decay times for the methyl deuteron signal in ME experiments was found to be almost one order of magnitude longer than the decay times of the single-quantum coherences (Table 2). Hence, although in more favorable circumstances (isolated deuterons) the DQ PGSE method could provide more effective gradient encoding in a diffusion experiment (*19–22*), the fast decay of the DQ coherences leads to that the DQ PGSE method does not produce any advantage in measuring the diffusion in the present sample.

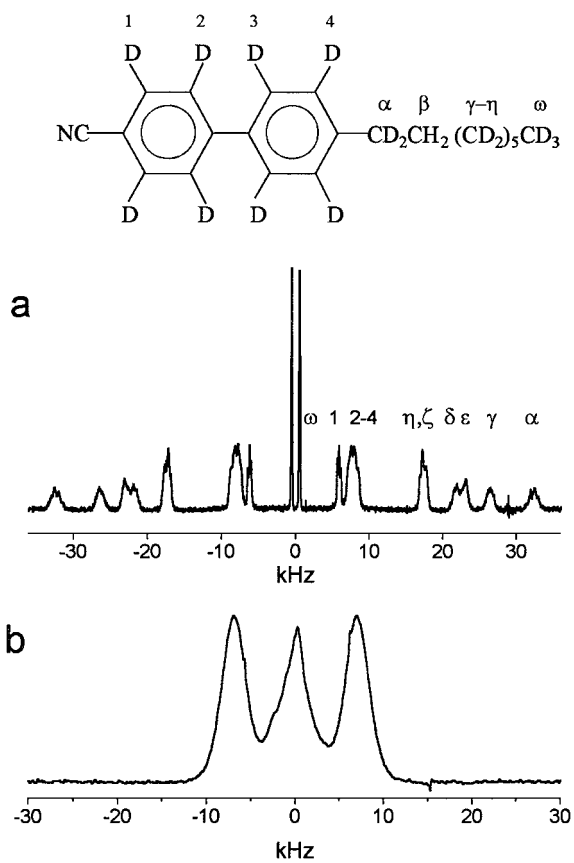

FIG. 2. (a) 31 MHz ^{2}H NMR and (b) 200 MHz ^{1}H NMR spectra of a partially deuterated 8CB sample in its smectic phase at 300 K. The liquid crystal sample is uniformly oriented by the magnetic field with its director parallel to the field direction.

TABLE 1
Relaxation Times in 8CB in its Nematic Phase at 307 K

Time constant (ms)	Deuterium position							
	ω	1	2–4	η,ζ	δ	ε	γ	α
T_1	294	8.5	8.7	56	28	30	20	12.6
T_{2SQ}[a]	4.2	0.97	0.86	2.0	1.2	1.2	1.0	0.75

[a] From the decay of single-quantum coherences.

TABLE 2
Relaxation Times for the ^{2}H Signal of the Methyl Group (ω) in 8CB at Different Temperatures

Time constant, ms	307 K nematic	295 K smectic A	285 K smectic A
T_1	294	200	143
T_{2SQ}[a]	4.2	3.2	2.9
T_{2DQ}[b]	1.7	1.0	0.9
T_{2ME}[c]	36.2	19.8	16.8

[a] From the decay of single-quantum coherences.
[b] From the decay of double-quantum coherences.
[c] From the decay of the magic-echo signal.

Measurement of Diffusion

With our current gradient setup (see below) having a maximum gradient strength of 300 G/cm, and with the diffusion coefficient of 8CB being on the order of 10^{-11} m^2/s, a diffusion experiment can be performed only by the methyl deuterons that have the longest relaxation times. Since $T_1 \gg T_2$ (Table 1) the PGSTE method is feasible as will be demonstrated below.

At higher temperatures where T_{2SQ} is sufficiently long one can make use of the ^{2}H PGSTE experiment without ME decoupling. In Fig. 3, we show the intensity of the methyl signal obtained by the PGSTE sequence in Fig. 1a applied to 8CB in its nematic phase at 307 K. With the diffusion time Δ set to 50 ms, the applied gradient $g = 20$ G/cm results in a complete coherence dephasing during the evolution time τ (achieved if $\tau > 2\pi/\gamma g l \approx 0.2$ ms, where $l \approx 5$ mm is the sample length in the gradient direction) but is too weak to produce a significant diffusion damping. Hence, our theoretical predictions can be easily tested. As expected, the signal from the cosine sequence with pulse angles $\phi = \psi = 90^\circ$ is quadrupole-modulated irrespective of the gradient strength (Fig. 3a). On the other hand, with $\phi = \psi = 54.7^\circ$ the modulation is present in the absence of gradient but is suppressed by the gradient (Fig. 3b) and the relative signal intensities are, respectively, $\approx 2/3$ and $\approx 1/3$. The sine-modulated sequence also behaves as predicted (Figs. 3c, 3d). Finally, the phase cycle that combines the signal from the cosine and sine STE sequences with $\phi = \psi = 54.7^\circ$ (see Experimental below) suppresses the modulation irrespective of the applied gradient strength (Fig. 3e).

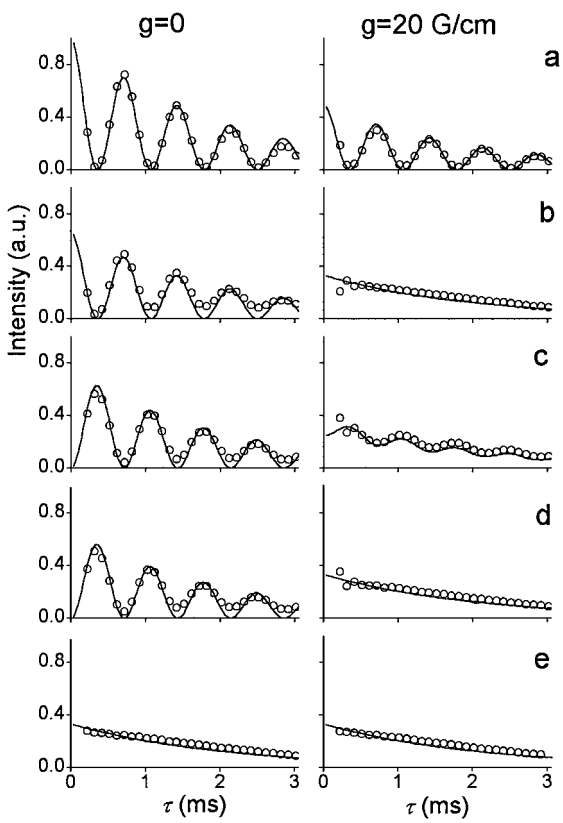

FIG. 3. Variation of the methyl signal intensity with increasing the delay τ in the ^{2}H PGSTE experiment in Fig. 1a applied to 8CB in its nematic phase at 307 K. The quadrupole splitting, which defines the observed modulation, has been measured to be 1.4 kHz. The field gradient g is applied parallel to the field direction. Left column: $g = 0$, right column: $g = 20$ G/cm. (a) Cosine sequence with $\phi = \psi = 90^\circ$. (b) Cosine sequence with $\phi = \psi = 54.7^\circ$. (c) Sine sequence with $\phi = \psi = 45^\circ$. (d) Sine sequence with $\phi = \psi = 54.7^\circ$. (e) combined cosine + sine sequence with $\phi = \psi = 54.7^\circ$. The solid lines are calculated using Eqs. [A6] and [A8] with the transverse relaxation introduced in a phenomenological way of multiplying the signal with $\exp(-2\tau/T_2)$ where $T_2 = 4.2$ ms (see Table 1).

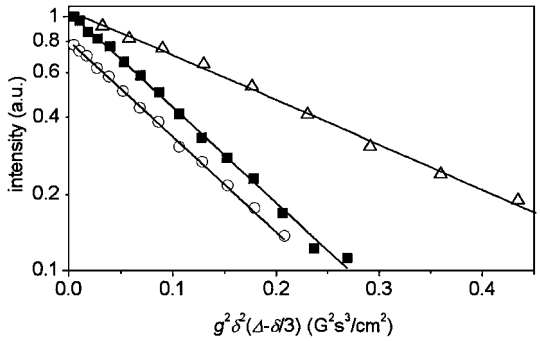

FIG. 4. The ^{2}H methyl signal intensity in 8CB versus $g^2\delta^2(\Delta - \delta/3)$ with increasing gradient strength obtained by the ^{2}H PGSTE experiment in Fig. 1a at 309 K in the nematic phase (squares) and by the ^{2}H PGSTE-ME experiment in Fig. 1b at 309 K in the nematic phase (circles, shifted down for clarity) and at 298 K in the smectic phase (triangles).

The results of the ^{2}H PGSTE NMR diffusion experiments in the nematic phase of 8CB at 309 K are shown in Fig. 4, with the signal intensities plotted versus $g^2\delta^2(\Delta - \delta/3)$ on a semi-logarithmic scale. Delays δ and Δ were set to 3 and 400 ms, respectively, and the field gradient, set to values up to 270 G/cm, was directed along the main magnetic field. The intensities were obtained by combining cosine and sine signals recorded with $\phi = \psi = 54.7^\circ$ (see Experimental). With 8 scans for each different gradient value and with a recycling delay of 2 s the total experimental time was about 3 min. The diffusion constant estimated by least-squares fitting Eqs. [1] and [6] to the decay in Fig. 4 is $D = (0.52 \pm 0.01) \times 10^{-10}$ m^2/s. The (random) error is estimated from the scatter of the experimental points around the fit.

At temperatures below 300 K, diffusion measurements by the STE sequence become difficult due to slow diffusion and short relaxation times. On the other hand, the PGSTE-ME sequence in Fig. 1b performs well at these temperatures. As shown in Table 2, the decay time of single-quantum coherences is prolonged by up to 9 times with ME. However, since only one-third of the evolution period is available for gradient pulses, the efficiency of gradient encoding increased only by a factor of $\sim 3^2$ (instead of $\sim 9^2$). To avoid excessive sample heating from the long RF pulses in the ME sandwich, the signal dependence on

the strength of the B_1 field during the lock pulses was examined. A significant decrease of the signal intensity was observed if B_1 was set below $\gamma B_1/2\pi = 4$ kHz. Hence, this value was chosen for the PGSTE-ME experiments, which, in combination with a recycling delay of 4 s, resulted in a moderate heating effect of about 0.5 K. The decay of the signal in a PGSTE-ME experiment with increasing gradient, recorded at temperature 298 K, is included in Fig. 4. The diffusion time Δ was fixed to 300 ms, while the total gradient time δ corresponded to 5.69 ms (with full evolution time $\tau = 19.8$ ms). With 8 accumulated transients for every gradient value, the observed decay is clearly Gaussian yielding $D = (0.232 \pm 0.007) \times 10^{-10}$ m^2/s. To compare the ^{2}H PGSTE and PGSTE-ME methods, the diffusion coefficient was measured using PGSTE-ME also at 309 K with Δ and δ set to 300 and 3.085 ms, respectively. With 4 accumulated transients and a recycling delay of 4 s, this experiment lasted 3 min, which is the same duration as that with PGSTE. The estimated diffusion coefficient $D = (0.512 \pm 0.007) \times 10^{-10}$ m^2/s agrees well with the PGSTE result presented above.

The diffusion coefficients measured by the ^{2}H PGSTE and PGSE-ME methods in a wide temperature range including the nematic and the smectic phases and for gradient directions parallel and perpendicular to the magnetic field are collected in Fig. 5. Moreover, results of diffusion measurement in the same sample by ^{1}H PGSTE NMR combined with homonuclear decoupling (*16*) are also shown in the Fig. 5. In general, excellent agreement between results obtained on different nuclei and by different methods can be observed.

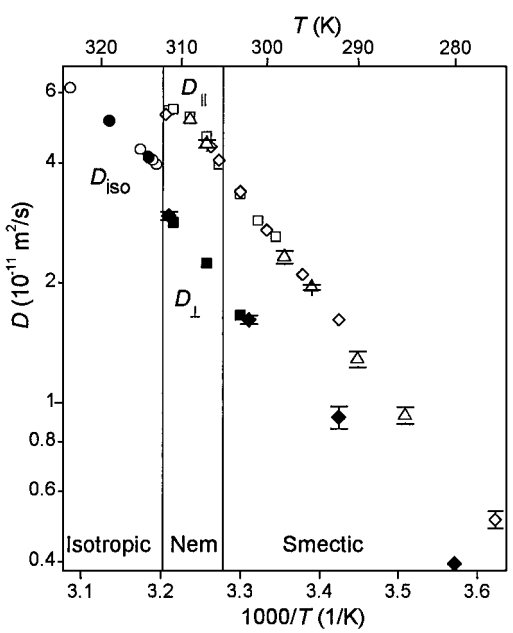

FIG. 5. The temperature dependence of the diffusion coefficients $D_\parallel$ (open symbols) and $D_\perp$ (solid symbols) in 8CB. The diffusion in nematic and smectic phases was measured by ^{2}H PGSTE (squares), ^{2}H PGSTE-ME (triangles), and by ^{1}H PGSTE with homonuclear decoupling (*16*) (diamonds). In the isotropic phase (circles) the conventional ^{2}H PGSTE technique was used.

CONCLUSION

As demonstrated above, ^{2}H PGSE NMR can, despite the low magnetogyric ratio of ^{2}H, be used for diffusion measurement in anisotropic liquid crystalline samples. In complete analogy to spin $I = \frac{1}{2}$ nuclei in isotropic liquids with relaxation times $T_1 \gg T_2$, STE-type ^{2}H PGSE sequences can access much lower diffusion coefficients than PGSE techniques based on solid/quadrupole echoes. An extra complication is the signal modulation by the quadrupolar interaction (also observed for spin $I > 1$ nuclei (*47*)), which, however, can be suppressed by setting the second and third RF pulses in the STE sequence to the magic angle 54.7° and by cycling the phase in an appropriate way. Further extension of the range of the accessible diffusion coefficients is achieved by using magic echo decoupling during the encoding/decoding periods of the PGSTE sequence. The resulting PGSTE-ME technique (*13*) is, however, more demanding on the NMR hardware and can also be prone to excessive sample heating by long RF irradiation. We also demonstrate that the PGSE method based on multiple-quantum coherences is less effective in the samples with simultaneous dipole and quadrupole couplings.

In the case of slow diffusion in anisotropic systems, ^{1}H (or ^{19}F) diffusion experiments combined with homonuclear decoupling are still the most sensitive and accurate (*16, 18, 48*) ones. For faster diffusion processes, however, the ^{2}H PGSTE and PGSTE-ME techniques can be simpler to implement since they have lower demands on the NMR hardware. Moreover, they do not involve the calibration of gradient scaling by homonuclear decoupling (*16*), and therefore, the obtained diffusion coefficients are subject to one less potential source of systematic error. Our results demonstrate that diffusion coefficients on the order of 10^{-11} m^2/s can be readily measured in deuterated liquid crystals.

Self-diffusion coefficients measured by deuterium PGSE NMR are, to our knowledge, the first of its kind in the thermotropic liquid crystals, although several different ^{1}H NMR approaches (see Ref. (*49*) for references) were already explored for the same purpose. One interesting conclusion we can draw from the data is that the self-diffusion coefficients in 8CB continuously change from the nematic to the smectic phase and diffusion is slower along the layers in the smectic phase than perpendicular to them in the whole temperature of range of the mesophase. Previously, this behavior has only been observed indirectly by guest molecules (*50, 51*). More detailed data in the present and in other liquid crystals will be communicated elsewhere.

EXPERIMENTAL

A partially deuterated 8CB sample has been synthesized according to procedure described earlier (*52*). This compound exhibits the following phase sequence: solid—smectic A—nematic—isotropic. The isotropic–nematic and nematic–smectic phase transition temperatures were determined from the

^{2}H spectrum to 312 and 305 K, respectively, in agreement with the results from literature (*53*). The nematic phase director orients parallel to the external magnetic field and keeps oriented while cooling to the smectic phase.

The measurements were performed on a Bruker DMX 200 spectrometer, operating at 31 MHz for deuterium. We used a homebuilt probe whose exchangeable gradient setup includes quadrupole gradient coils with gradient directions parallel or perpendicular to the static magnetic field as described previously (*25*). The RF coil is a solenoid of 6 mm i.d. and 2 cm length, made of 40 turns of copper wire. With about 300 W RF power, the length of the ^{2}H 90° pulses was 5 μs. The sample resided in a 5-mm o.d. and 15-mm-long sealed glass ampule. The current into the gradient coils was supplied by a Bruker BAFPA-40 current generator. The gradient strength was calibrated by measuring the diffusion coefficient of heavy water at 25°C and comparing that to the literature value $D = 1.872 \times 10^{-9}$ m^2/s (*54*). The phase cycle for the STE sequence of Fig. 1a was {first pulse + $y, -y$; second and third pulses $2(+y)$, $2(-x)$, $2(-y)$, $2(+x)$; receiver $-x$, $2(+x)$, $2(-x)$, $2(+x)$, $-x$}. For the PGSTE-ME sequence the RF phases in magic echo sandwich were as shown in Fig. 1b, while the phases of stimulated echo pulses were cycled as {first pulse $+y, -y$; second and third pulses $2(+y)$, $2(-y)$} with the receiver phase set to $\{+x, -x\}$. The ^{1}H diffusion experiment was performed as described in (*16*).

The average temperature was observed and regulated with an accuracy of 0.1 K by the Bruker BVT-3000 unit supplied with the spectrometer. The temperature shift and temperature gradient within the sample caused by the RF irradiation in the PGSTE-ME experiment was calibrated by observing the changes in the splitting and broadening of the ^{2}H NMR spectra.

APPENDIX

The spin dynamics in the sequence of Fig. 1a with spin interactions governed by the Hamiltonian of Eq. [2] for cosine- and sine-modulated signal is calculated under the assumption of perfectly hard RF pulses with 90° pulse angle for the first pulse, and with arbitrary ϕ and ψ pulse angles for the second and third pulses, respectively. Transverse relaxation during evolution periods of length τ is neglected while the t_m period is assumed to be long enough $t_m \gg T_2$ to suppress all coherences just before the third pulse. Hence, only Zeeman and quadrupolar orders at that point contribute to the final signal. It is also assumed that any possible contribution from longitudinal magnetization, created by spin relaxation during t_m, is eliminated by an appropriate phase cycle (*27*). We limit our attention here to a homogeneously oriented sample with a single quadrupole frequency of ω_Q.

The density matrix in the rotating frame immediately after second pulse in the sequence of Fig. 1a is proportional to

$$\sigma(\tau) \propto \exp(-i\phi I_\beta)\exp(-iH\tau)\exp(-i\pi/2\, I_\alpha) I_z \times \exp(i\pi/2\, I_\alpha)\exp(iH\tau)\exp(i\phi I_\beta) \quad [A1]$$

with $\alpha, \beta = x, y$ and H given in Eq. [2]. It can be readily calculated by using the standard formalism summarized, e.g., in (*27*). The evaluation of Eq. [A1] for the cosine sequence with the RF phases set to $\{+y, \pm y$, and $\pm y\}$ yields at the end of the t_m period

$$\sigma(\tau + t_m) \propto \pm\Big[-\sin\phi \times \cos(\omega_Q\tau)\cos(\omega_1\tau) \times \exp(-t_m/T_{1Z}) \times I_z + \frac{3}{2}\sin 2\phi \times \sin(\omega_Q\tau)\sin(\omega_1\tau) \times \exp(-t_m/T_{1Q})\big(I_z{}^2 - 2/3\big)\Big]. \quad [A2a]$$

Similarly, for the sine sequence with RF phases set to $\{+y, \pm x$, and $\pm x\}$ we obtain

$$\sigma(\tau + t_m) \propto \pm\Big[\sin\phi \times \cos(\omega_Q\tau)\sin(\omega_1\tau) \times \exp(-t_m/T_{1Z}) \times I_z + \frac{3}{2}\sin 2\phi \times \sin(\omega_Q\tau)\cos(\omega_1\tau) \times \exp(-t_m/T_{1Q}) \times \big(I_z{}^2 - 2/3\big)\Big]. \quad [A2b]$$

The first and second terms in Eqs. [A2] correspond to Zeeman and quadrupolar orders, respectively, which decay with their respective time constants T_{1Z} and T_{1Q}.

The density matrix at the time τ after the last pulse is given by

$$\sigma(\tau + t_m + \tau) \propto \exp(-iH\tau)\exp(-i\psi I_\alpha)\sigma(\tau + t_m) \times \exp(i\psi I_\alpha)\exp(iH\tau). \quad [A3]$$

The evaluation of this expression with $\sigma(\tau + t_m)$ from Eq. [A2] and taking the traces $\mathrm{Tr}\{[I_x + iI_y] \times \sigma(\tau + t_m + \tau)\}$ produces the complex transverse magnetization for the cosine sequence in the form

$$A_c = -A_c^{(0)} \times \cos^2(\omega_Q\tau) \times \cos(\omega_1\tau) \times \exp(i\omega_2\tau - t_m/T_{1Z}) + i \times A_s^{(0)} \times \sin^2(\omega_Q\tau) \times \sin(\omega_1\tau) \times \exp(i\omega_2\tau - t_m/T_{1Q}) \quad [A4a]$$

and for the sine sequence

$$A_s = -i \times A_c^{(0)} \times \cos^2(\omega_Q\tau) \times \sin(\omega_1\tau) \times \exp(i\omega_2\tau - t_m/T_{1Z}) + A_s^{(0)} \times \sin^2(\omega_Q\tau) \times \cos(\omega_1\tau) \times \exp(i\omega_2\tau - t_m/T_{1Q}). \quad [A4b]$$

Here, the time-independent coefficients are

$$A_c^{(0)} = \sin\phi\sin\psi, \quad [A5a]$$

$$A_s^{(0)} = \frac{3}{4}\sin(2\phi)\sin(2\psi). \quad [A5b]$$

Both signals of Eqs. [A4] are modulated by (twice) the quadrupole frequency and the spatially dependent frequency offset is encoded in the phase shifts $(\omega_1\tau)$ and $(\omega_2\tau)$.

For on-resonance ($g = 0$), Eqs. [A4] converge to the familiar expressions (*26*)

$$A_c = A_c^{(0)} \cos^2(\omega_Q \tau) \times \exp(-t_m/T_{1Z}), \quad [A6a]$$

$$A_s = A_s^{(0)} \sin^2(\omega_Q \tau) \times \exp(-t_m/T_{1Q}), \quad [A6b]$$

and maximum signals $A_c = 1$ and $A_s = 3/4$ are obtained for the cosine and sine parts with the flip angles set to $\phi = \psi = 90^\circ$ and $\phi = \psi = 45^\circ$, respectively, and with $\tau = k\pi/\omega_Q$ and $\tau = (k\pi + \pi/2)/\omega_Q$, respectively ($k = 0, 1, 2, \ldots$).

To calculate the signal of Eqs. [A4] in the presence of field gradients the integral over the sample volume must be calculated. It is instructive to consider first the case of the gradient g resulting in complete coherence dephasing during τ but being too weak to produce a significant diffusion effect. Consequently, with $\omega = \omega_1 = \omega_2$ the averaging yields

$$\langle \cos(\omega\tau) \sin(\omega\tau) \rangle \approx 0, \quad [A7a]$$

$$\langle \cos(\omega\tau) \cos(\omega\tau) \rangle \approx \langle \sin(\omega\tau) \sin(\omega\tau) \rangle \approx 1/2, \quad [A7b]$$

which results in the signal

$$A_c = -A_s = -1/2\big[A_c^{(0)} \cos^2(\omega_Q \tau) \times \exp(-t_m/T_{1Z}) + A_s^{(0)} \sin^2(\omega_Q \tau) \times \exp(-t_m/T_{1Q})\big]. \quad [A8]$$

For the particular case of $\phi = \psi = 45^\circ$ the same results has been obtained in (*55*). For long relaxation times $T_{1Z}, T_{1Q} \gg t_m$ the maximum signal

$$A_c = -A_s = -\frac{1}{2} \quad [A9]$$

is obtained with the flip angles $\phi = \psi = 90^\circ$ and with delay $\tau = k\pi/\omega_Q$ ($k = 0, 1, 2, \ldots$). Thus, only one half of initial transverse magnetization after the first pulse is recovered, as expected for the stimulated echo.

Quadrupolar modulation during τ in Eq. [A8] can be avoided (again, under the assumption of slow relaxation) by setting the pulse angles to the magic angle $\phi = \psi = 54.7^\circ$, which results in $A_c^{(0)} = A_s^{(0)} = \frac{2}{3}$ and, hence,

$$A_c = -A_s = -\frac{1}{3} \quad [A10]$$

at any τ. This feature, however, has been achieved at the expense of a somewhat reduced (by a factor of $\frac{2}{3}$) signal intensity. More importantly, the modulation is still present at low or vanishing field gradient values, which could disturb the diffusion experiment.

Suppressing of quadrupolar modulation at an arbitrary field gradient is achieved by combining the two signals of Eq. [A4]. Indeed, with $\phi = \psi = 54.7^\circ$ the difference signal $A = A_s - A_c$ becomes

$$A = A_s - A_c = \frac{2}{3}[\cos^2(\omega_Q \tau) \exp(-t_m/T_{1Z}) + \sin^2(\omega_Q \tau) \times \exp(-t_m/T_{1Q})] \exp(i(\omega_2 - \omega_1)\tau), \quad [A11]$$

which, in the limit of long relaxation times $T_{1Z}, T_{1Q} \gg t_m$, yields

$$A = \frac{2}{3} \exp[i(\omega_2 - \omega_1)\tau]. \quad [A12]$$

Hence, the quadrupolar modulation vanishes and the signal is solely determined by the evolution under the frequency offset.

ACKNOWLEDGMENTS

This work has been supported by the Carl Tryggers Foundation, the Swedish Natural Science Research Council (NFR), and the Deutscher Academischer Austauschdienst together with the Swedish Institute under Project 313-S-PPP-7/98.

REFERENCES

1. E. O. Stejskal and J. E. Tanner, Spin diffusion measurements: Spin echoes in the presence of a time-dependent field gradient, *J. Chem. Phys.* **42,** 288–292 (1965).
2. J. E. Tanner, Use of the stimulated echo in NMR diffusion studies, *J. Chem. Phys.* **52,** 2523–2526 (1970).
3. P. Stilbs, Fourier transform pulsed-gradient spin-echo studies of molecular diffusion, *Prog. Nucl. Magn. Reson. Spectrosc.* **19,** 1–45 (1987).
4. P. T. Callaghan, "Principles of Nuclear Magnetic Resonance Microscopy," Clarendon Press, Oxford (1991).
5. W. S. Price, Pulsed-field gradient nuclear magnetic resonance as a tool for studying translational diffusion: Part I. Basic theory, *Concepts Magn. Reson.* **9,** 299–336 (1997).
6. W. S. Price, Pulsed-field gradient nuclear magnetic resonance as a tool for studying translational diffusion: Part II. Experimental aspects, *Concepts Magn. Reson.* **10,** 197–237 (1998).
7. R. Kimmich and E. Fischer, One- and two-dimensional pulse sequences for diffusion experiments in the fringe field of superconducting magnets, *J. Magn. Reson. A* **106,** 229–235 (1994).
8. R. Kimmich, W. Unrath, G. Schnur, and E. Rommel, NMR measurement of small self-diffusion coefficients in the fringe field of superconducting magnets, *J. Magn. Reson.* **91,** 136–140 (1991).
9. I. Chang, F. Fujara, B. Geil, G. Hinze, H. Sillescu, and A. Tölle, New perspectives of NMR in ultrahigh static magnetic field gradients, *J. Non-Cryst. Solids* **172–174,** 674–681 (1994).
10. B. Geil, Measurement of translational molecular diffusion using ultrahigh magnetic field gradient NMR, *Concepts Magn. Reson.* **10,** 299–321 (1998).
11. I. Chang, G. Hinze, G. Diezemann, F. Fujara, and H. Sillescu, Self-diffusion coefficient in plastic crystals by multiple-pulse NMR in large static field gradients, *Phys. Rev. Lett.* **76,** 2523–2526 (1996).
12. I. Chang, G. Diezemann, G. Hinze, R. Böhmer, and H. Sillescu, Far-off-resonance averaging of dipolar interactions in solids, *J. Magn. Reson.* **124,** 165–171 (1997).
13. W. Zhang and D. G. Cory, First direct measurement of the spin diffusion rate in a homogeneous solid, *Phys. Rev. Lett.* **80,** 1324–1327 (1998).

14. W. Zhang and D. G. Cory, Pulsed gradient NMR probes for solid state studies, *J. Magn. Reson.* **132,** 144–149 (1998).
15. S. V. Dvinskikh, R. Sitnikov, and I. Furó, ^{13}C PGSE NMR experiment with heteronuclear dipolar decoupling to measure diffusion in liquid crystals and solids, *J. Magn. Reson.* **142,** 102–110 (2000).
16. S. V. Dvinskikh and I. Furó, Combining PGSE NMR with homonuclear dipolar decoupling, *J. Magn. Reson.* **144,** 142–149 (2000).
17. S. V. Dvinskikh and I. Furó, Cross-relaxation effects in stimulated-echo-type PGSE NMR experiments by bipolar and monopolar gradient pulses, *J. Magn. Reson.* **146,** 283–289 (2000).
18. S. V. Dvinskikh and I. Furó, Measurement of the principal values of the anisotropic diffusion tensor in an unoriented sample by exploiting the chemical shift anisotropy: ^{19}F PGSE NMR with homonuclear decoupling, *J. Magn. Reson.* **148,** 73–77 (2001).
19. J. F. Martin, L. S. Selwyn, R. R. Vold, and R. L. Vold, The determination of translational diffusion constants in liquid crystals from pulsed field gradient double quantum spin echo decays, *J. Chem. Phys.* **76,** 2632–2634 (1982).
20. D. Zax and A. Pines, Study of anisotropic diffusion of oriented molecules by multiple quantum spin echoes, *J. Chem. Phys.* **78,** 6333–6334 (1983).
21. L. E. Kay and J. H. Prestegard, An application of pulse-gradient double-quantum spin echoes to diffusion measurements on molecules with scalar-coupled spins, *J. Magn. Reson.* **67,** 103–113 (1986).
22. L. v. Dam, B. Andreasson, and L. Nordenskiöld, Multiple-quantum pulsed gradient NMR diffusion experiments on quadrupolar ($I > 1/2$) spins, *Chem. Phys. Lett.* **262,** 737–743 (1996).
23. P. T. Callaghan, M. A. Le Gros, and D. N. Pinder, The measurement of diffusion using deuterium pulsed field gradient nuclear magnetic resonance, *J. Chem. Phys.* **79,** 6372–6381 (1983).
24. H. Jóhannesson, I. Furó, and B. Halle, Orientational order and micelle size in the nematic phase of the cesium pentadecafluorooctanoate-water system from the anisotropic self-diffusion of water, *Phys. Rev. E* **53,** 4904–4917 (1996).
25. I. Furó and H. Jóhannesson, Accurate anisotropic water-diffusion measurements in liquid crystals, *J. Magn. Reson. A* **119,** 15–21 (1996).
26. C. Schmidt, B. Blümich, and H. W. Spiess, Deuteron two-dimensional exchange NMR in solids, *J. Magn. Reson.* **79,** 269–290 (1988).
27. K. Schmidt-Rohr and H. W. Spiess, "Multidimensional Solid-State NMR and Polymers," Academic Press, London (1994).
28. W.-K. Rhim, A. Pines, and J. S. Waugh, Time-reversal experiments in dipolar-coupled spin systems, *Phys. Rev. B* **3,** 684–696 (1971).
29. R. Kimmich, J. Niess, and S. Hafner, Quadrupolar magic echoes, *Chem. Phys. Lett.* **190,** 503–506 (1992).
30. S. Matsui, Solid-state NMR imaging by magic sandwich echoes, *Chem. Phys. Lett.* **179,** 187–190 (1991).
31. D. E. Demco, S. Hafner, and R. Kimmich, Spatially resolved homonuclear solid-state NMR. III. Magic-echo and rotary-echo phase-encoding imaging, *J. Magn. Reson.* **96,** 307–322 (1992).
32. M. A. Hepp and J. B. Miller, Mapping molecular orientation by solid-state NMR imaging, *J. Magn. Reson. A* **111,** 62–69 (1994).
33. S. Hafner, D. E. Demco, and R. Kimmich, Magic echoes and NMR imaging of solids, *Solid State Nucl. Magn. Reson.* **6,** 275–293 (1996).
34. R. Kimmich, "NMR Tomography, Diffusometry, Relaxometry," Springer-Verlag, Berlin (1997).
35. D. E. Demco and B. Blümich, Solid-state NMR imaging methods. Part II: Line narrowing, *Concepts Magn. Reson.* **12,** 269–288 (2000).
36. N. Boden, L. D. Clark, R. J. Bushby, J. W. Emsley, G. R. Luckhurst, and C. P. Stockley, A deuterium NMR study of chain ordering in the liquid crystals 4,4′-di-n-heptyloxyazoxybenzene and 4-n-octyl-4′-cyanobiphenyl, *Mol. Phys.* **42,** 565–594 (1981).
37. D. Sandström and H. Zimmermann, Correlation of deuterium quadrupolar couplings and carbon-13 chemical shifts in ordered media by multiple-quantum NMR, *J. Phys. Chem. B* **104,** 1490–1493 (2000).
38. J. H. Davis, K. R. Jeffrey, M. Bloom, M. I. Valic, and T. P. Higgs, Quadrupolar echo deuteron magnetic resonance spectroscopy in ordered hydrocarbon chains, *Chem. Phys. Lett.* **42,** 390–394 (1976).
39. G. L. Hoatson and R. L. Vold, ^{2}H-NMR spectroscopy of solids and liquid crystals, *NMR Basic Principles Progr.* **32,** 1–67 (1994).
40. G. Bodenhausen, R. L. Vold, and R. R. Vold, Multiple quantum spin-echo spectroscopy, *J. Magn. Reson.* **37,** 93–106 (1980).
41. R. L. Vold, R. R. Vold, R. Poupko, and G. Bodenhausen, The determination of all six spectral densities of motion for partially oriented dichloromethane-d_2, *J. Magn. Reson.* **38,** 141–161 (1980).
42. I. Furó and B. Halle, Multiple quantum NMR spectroscopy on $I > 1$ nuclei in anisotropic systems, *Molec. Phys.* **76,** 1169–1197 (1992).
43. R. R. Vold, Nuclear spin relaxation, *in* "Nuclear Magnetic Resonance of Liquid Crystals" (J. W. Emsley, Eds.), pp. 253–288, Reidel, Dordrecht (1985).
44. R. Poupko, R. L. Vold, and R. R. Vold, Density matrix calculations of the relaxation of two deuterons in an ordered medium, *J. Magn. Reson.* **34,** 67–81 (1979).
45. D. Jaffe, R. L. Vold, and R. R. Vold, Deuterium relaxation of a partially oriented methyl group. II. Density matrix calculations of multiple quantum spin-echo linewidths, *J. Magn. Reson.* **46,** 496–502 (1982).
46. O. Kircher, G. Diezemann, R. Böhmer, G. Hinze, K. U. Schug, H. Sillescu, and H. Zimmermann, Decay of single and double quantum coherences in deuterated glassy ortho-terphenyl, *J. Chem. Phys.* **108,** 8550–8556 (1998).
47. R. Böhmer, Multiple-time correlation functions in spin-3/2 solid-state NMR spectroscopy, *J. Magn. Reson.* **147,** 78–88 (2000).
48. S. V. Dvinskikh and I. Furó, Anisotropic self-diffusion in the nematic phase of a thermotropic liquid crystal by ^{1}H spin-echo nuclear magnetic resonance, *J. Chem. Phys.* **115,** 1946–1950 (2001).
49. G. J. Krüger, Diffusion in thermotropic liquid crystals, *Phys. Rep.* **82,** 229–269 (1982).
50. M. Hara, H. Takezoe, and A. Fukuda, Forced Rayleigh scattering in nCB's ($n = 5$–9) with methyl red and binary mass diffusion constants, *Jpn. J. Appl. Phys.* **25,** 1756–1761 (1986).
51. J. K. Moscicki, Y.-K. Shin, and J. H. Freed, Translational diffusion in a smectic-A phase by electron spin resonance imaging: the free-volume model, *J. Chem. Phys.* **99,** 634–649 (1993).
52. H. Zimmermann, Specifically deuterated intermediates for the synthesis of liquid crystals and liquid-crystalline polymers, *Liq. Cryst.* **4,** 591–618 (1989).
53. J. W. Emsley, G. R. Luckhurst, and P. Pedrielli, Magnetic field induced alignment of the director in a smectic A phase: Surface effects, *Chem. Phys. Lett.* **320,** 255–261 (2000).
54. R. Mills, Self-diffusion in normal and heavy water in the range 1–45°, *J. Phys. Chem.* **77,** 685–688 (1973).
55. S. B. Ahmad and K. J. Packer, Nuclear magnetic relaxation in spin-1 systems: The response to three-pulse sequence II. Inhomogeneous B_0 field, *Mol. Phys.* **37,** 59–71 (1979).